



NONLINEARITIES IN GENERALIZED AERODYNAMIC FORCES IN THE CONTEXT OF T-TAIL FLUTTER

Dominik Schäfer¹

¹German Aerospace Center (DLR), Institute of Aeroelasticity, Bunsenstrasse 10, 37073 Göttingen (Germany)
email: d.schaefer@dlr.de

Abstract

Assessment of T-tail flutter requires unsteady aerodynamic forces beyond the scope of the conventional DLM, usually accounted for by means of correctional terms computed by external methods and superposed with the DLM aerodynamics. The increasingly employed CFD methods as high-fidelity alternatives to potential flow solutions inherently capture the aerodynamic forces to their full extent. However, literature has shown that the full description of the unsteady aerodynamic terms in combination with a linear modal approach for the representation of the dynamical system of T-tails may lead to spurious stiffness terms. For a physically more accurate flutter assessment, it is suggested to include quadratic deformation components in the modal representation. While the effect of higher order deformation components on the stiffness of the vertical tail plane out-of-plane bending mode shape is known from literature, their impact on the aerodynamic coupling terms has not been studied in depth so far. As these are driving factors for flutter, this paper works out the impact of quadratic mode shape components on the aerodynamic coupling terms with regard to frequency of oscillation and deformation amplitude.

The two mode shapes studied in this paper are vertical tail plane out-of-plane bending and torsion. Both mode shapes are approximated as rigid body rotations of the horizontal tail plane w.r.t. the longitudinal and vertical axes, respectively. This allows for an analytical description of the linear and quadratic deformations. In order to exclude aerodynamic interference between horizontal and vertical tail plane, only the isolated horizontal tail plane is studied. The aerodynamics is restricted to inviscid flow at a Mach number of 0.4 and atmospheric conditions at mean sea level according to the International Standard Atmosphere. Converged solutions to harmonic excitation of the geometry's CFD surface mesh are studied which enables the evaluation of aerodynamic stiffness and damping from magnitude and phase angle of the input and output signals. Fourier transformation of the signals as well as a curve fitting approach is used to address the frequency content of the aerodynamic response.

The impact of the quadratic mode shape components is most notable for the aerodynamic influence of the horizontal tail plane roll motion on itself and on the yaw motion. Here, the change in stiffness regarding the roll motion, as outlined above, is observed as well as a striking impact on the stiffness and damping regarding the yaw motion, i.e. the aerodynamic coupling term at non-infinitesimal deformation amplitudes. Concerning the yaw motion, the quadratic deformation components affect the stiffness of the aerodynamic influence on itself. The damping terms, however, are insensitive to the quadratic deformation components.

For the amplitude dependency, a nonlinearity in the coupling term of horizontal tail plane roll motion on yaw motion is identified, which is fundamentally different between a linear and a quadratic deformation approach. In addition, a third harmonic content in the generalized aerodynamic forces is observed. All other aerodynamic terms behave linearly w.r.t. the deformation amplitude.

Keywords: Aeroelasticity, T-tail flutter, Quadratic mode shape components, CFD unsteady aerodynamics, Nonlinear dynamics

1. Introduction

For numerical T-tail flutter studies, unsteady aerodynamic forces beyond the scope of the conventional DLM are required. External aerodynamic methods based on strip theory are a feasible way of

computing the additional terms and superposing them with the DLM aerodynamics [1–3]. Albeit its simplicity, the derivation of an additional computational mesh from the DLM mesh is a disadvantage of this method, as it is error prone and introduces a further discretization error. Enhanced DLM algorithms [4] or UVLM [5] are two comprehensive low- to mid-fidelity approaches without the necessity of superposing externally computed aerodynamic forces. For increased fidelity, especially in transonic flow conditions, CFD methods may be applied for the study of T-tail flutter [6–10]. While these approaches feature a comprehensive description of the aerodynamic terms required for accurate T-tail flutter assessment, literature has shown that the structural displacements need to be described geometrically nonlinear in order to avoid spurious stiffness terms in the vertical tail plane (VTP) bending mode shape [4]. This may be achieved by using an extended modal approach with quadratic mode shape components.

The concept of quadratic mode shape components has been introduced by Segalman and Dohrmann for rotating flexible structures in [11–15]. In their works, they propose a series of nonlinear static finite element analyses to obtain the quadratic mode shape components. Ritter uses this idea for simulating the nonlinear aeroelastic gust responses of free-flying aircraft in [16]. Van Zyl seized upon the subject of quadratic mode shape components for T-tail flutter studies and proposes a method for computing the quadratic mode shape components based on linear finite element analyses [17]. This approach has the advantage of a significant reduction in computational time, as only one static finite element analysis is required for the computation of one quadratic mode shape component as opposed to the nonlinear finite element approach, which requires a large number of nonlinear finite element analysis runs for each component. The linear approach has been applied most recently to T-tail flutter simulations by Murua in combination with potential flow theory based aerodynamics [5], by Farao et al. for the simulation of nonlinear gust response of a full aircraft model [18] and by Schäfer for T-tail flutter simulations in combination with linearized frequency domain CFD aerodynamics [19]. Regarding T-tail flutter mechanisms, typically VTP out-of-plane bending and torsion are the most relevant linear structural mode shapes. The VTP out-of-plane bending implicates a roll motion of the horizontal tail plane (HTP) and the VTP torsion results in an HTP yaw motion. The quadratic deformation components of the two mode shapes may be described as a spanwise shortening of VTP and HTP for the VTP out-of-plane bending deformation and a spanwise shortening of the HTP for the VTP torsion, see Figure 1. Here, the blue surface color illustrates the linear mode shapes and the orange surface color the quadratic deformation. Note that the surface of the deformed geometry in the VTP's torsional mode shape, Figure 1b, is artificially elevated slightly in vertical direction for the case with quadratic deformation in order to make the quadratic deformation component more perceptible.

To address the shortcoming of a commonly used linear modal approach for flutter assessment of T-tail configurations, the quadratic deformation components of the mode shapes under consideration are usually computed numerically as in [13, 16, 17, 19] and, together with the steady aerodynamic forces, an additional stiffness matrix is constructed and superposed with the structural stiffness. For increasing deformation amplitudes, however, the effect of higher order deformation components on the aerodynamic response is unknown, but knowledge about nonlinearities in a dynamical system is required to avoid detrimental oscillations which occur below the linear flutter boundary. The literature on T-tail flutter is currently limited to linear dynamics with a few exceptions regarding Limit Cycle Oscillations due to control surface freeplay using potential flow theory aerodynamics [20, 21]. It is expected, for example, that aerodynamic nonlinearities originate from induced drag components due to the roll motion of the HTP, which perform mechanical work on the VTP torsion and trigger aerodynamic coupling between the structural mode shapes. Figure 2 illustrates this conceivable possibility based on flow vorticity for an HTP roll motion at Mach 0.4 and reduced frequency of 0.231. The symmetric tip vortex of the undeformed model, Figure 2a, evolves to an asymmetric one when the HTP undergoes a roll motion, leading to an asymmetric induced drag component. Hence, it is expected that the fundamental mode shapes involved in T-tail flutter, namely VTP out-of-plane bending and torsion, induce aerodynamic stiffness and damping terms which are nonlinear with respect to the deformation amplitude. As the geometry changes when higher order deformation terms are included, it is further expected that the nonlinearities are fundamentally different between a

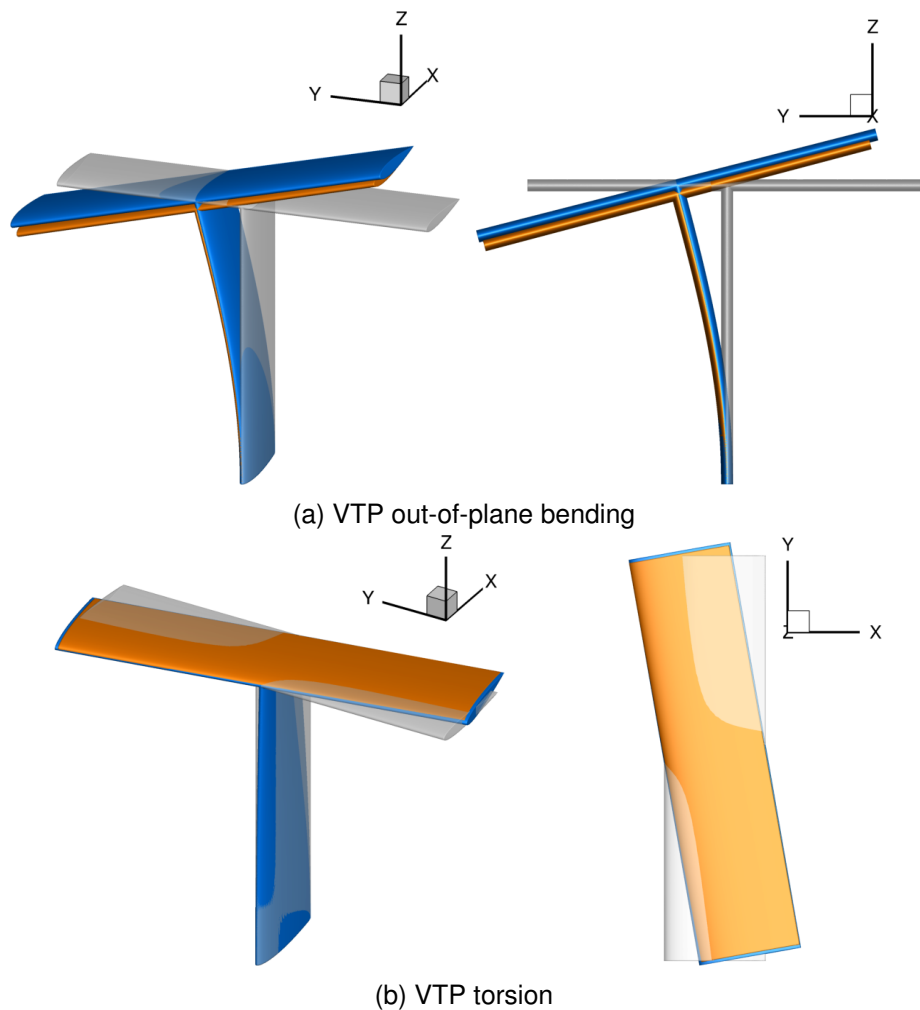


Figure 1 – Typical linear mode shapes (blue surface color) involved in T-tail flutter and the corresponding quadratic deformations (orange surface color)

linear and a nonlinear deformation model. Hence, for nonlinear flutter assessment, the use of a linear deformation model is insufficient. Based on these considerations, the impact of an extended modal representation of the dynamical system on T-tail flutter stability depending on deformation amplitude and oscillation frequency needs to be addressed.

2. Work Description

To study the effect of higher order deformation components on the response of aerodynamic forces on structural deformation, the focus is set on an isolated HTP in order to exclude aerodynamic interference effects from the studies. Furthermore, viscous effects are neglected. The structural mode shapes are approximated as rigid body rotations w.r.t. the longitudinal axis for the VTP out-of-plane bending and the vertical axis for the VTP torsion. This allows for a straightforward evaluation of the linear and quadratic deformation components from rotation matrices without the need of using a structural solver to compute the higher order deformation components. With this, errors in computation of the deformation components are avoided and the terms involved in the deformation process are explicitly defined. Harmonic excitation of the CFD surface mesh is used for computing the aerodynamic response at varying amplitudes and frequencies. The resulting time domain aerodynamic forces are generalized according to the linear and extended modal formulations and analyzed regarding aerodynamic stiffness and damping of the first harmonic content based on their magnitudes and phase angles. These values are obtained from both, applying a discrete Fourier transform (DFT) algorithm on the output signal and fitting a periodic function with multiples of the fundamental excitation frequency into the output signal for the selected time window. The DFT-approach may also be applied to pulse excitation to get the complex moduli for a range of reduced frequencies with a

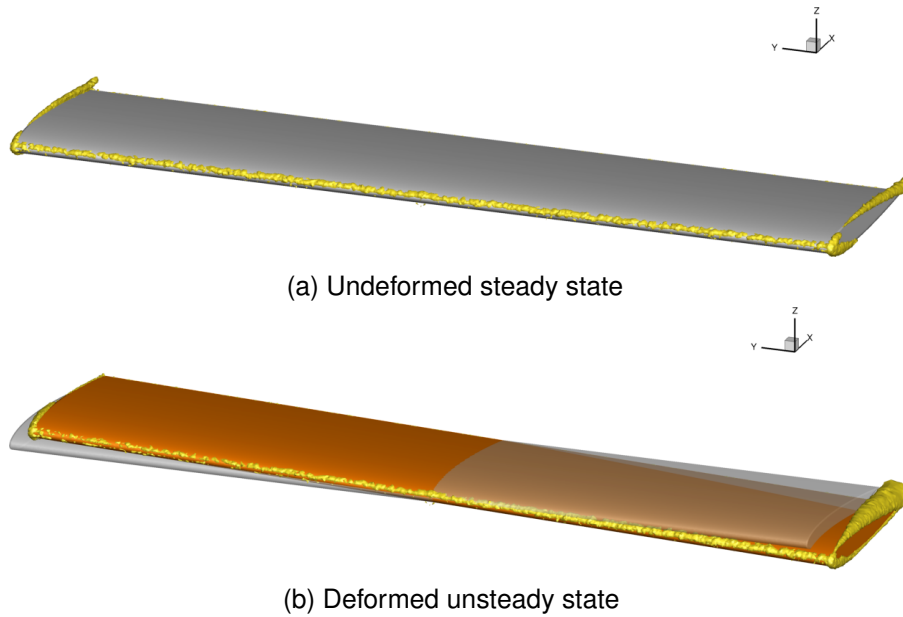


Figure 2 – Asymmetric vorticity geometry evolving from HTP roll motion

single simulation run. A sliding Fourier transform with a window size of two periods of oscillation is used to continue the simulation until the magnitudes of the target generalized aerodynamic forces (GAF) show a convergence with a residual of 0.1 % for a time span of two periods. A Cauchy convergence criterion is used on the lift force, drag force, and lateral moment coefficients with relative values of $1e-6$, $1e-6$, $5e-6$, respectively, for the inner CFD iterations at each physical time step. The Linearized Frequency Domain (LFD) approach [22], as a sophisticated way for obtaining the first harmonic content in GAF suitable for flutter prediction of complex configurations, serves as reference in this work for the chosen approach for computing frequency domain GAFs from time domain signals at small amplitudes.

3. Methods

3.1. Deformation Description

The approximation of the structural mode shapes by rigid body rotations is described here exemplarily for the roll motion. The approach allows for an analytical description of the deformation using the nonlinear rotation matrix with roll angle φ

$$\mathbf{R} = \begin{bmatrix} 1 & 0 & 0 \\ 0 & \cos(\varphi) & -\sin(\varphi) \\ 0 & \sin(\varphi) & \cos(\varphi) \end{bmatrix} \quad (1)$$

Expanding the sine and cosine terms in Eq. 1 as Taylor series with collected higher order terms (H.O.T) [23]

$$\sin(\varphi) \approx \varphi - \frac{\varphi^3}{3!} + \text{H.O.T} \quad (2)$$

$$\cos(\varphi) \approx 1 - \frac{\varphi^2}{2!} + \text{H.O.T} \quad (3)$$

and truncating them after the first and second order terms, respectively, leads to the linear (Eq. 4,

superscript $()^{(1)}$ and the quadratic (Eq. 5, superscript $()^{(2)}$) rotation matrices.

$$\mathbf{R}^{(1)} = \begin{bmatrix} 1 & 0 & 0 \\ 0 & 1 & -\varphi \\ 0 & \varphi & 1 \end{bmatrix} \quad (4)$$

$$\mathbf{R}^{(2)} = \begin{bmatrix} 1 & 0 & 0 \\ 0 & 1 - 1/2\varphi^2 & -\varphi \\ 0 & \varphi & 1 - 1/2\varphi^2 \end{bmatrix} \quad (5)$$

3.2. GAF Evaluation from Time Domain CFD Computations

For evaluating GAFs from time domain CFD results, the extended modal formulation used in this work reads [16]

$$Q = \boldsymbol{\phi}^{(1)T} \mathbf{f} + \boldsymbol{\phi}^{(2)T} \mathbf{f}_q \quad (6)$$

Here, $\boldsymbol{\phi}^{(1)}$ and $\boldsymbol{\phi}^{(2)}$ denote the linear mode shape and the quadratic mode shape components vector, respectively. In case of the roll deformation, these terms become

$$\boldsymbol{\phi}^{(1)} = \frac{\partial \mathbf{R}^{(1)}}{\partial \varphi} \mathbf{x} \quad (7)$$

and

$$\boldsymbol{\phi}^{(2)} = \frac{\partial^2 \mathbf{R}^{(2)}}{\partial \varphi^2} \mathbf{x} \quad (8)$$

with

$$\frac{\partial \mathbf{R}^{(1)}}{\partial \varphi} \mathbf{x}_i = \begin{bmatrix} 0 & 0 & 0 \\ 0 & 0 & -1 \\ 0 & 1 & 0 \end{bmatrix} \mathbf{x}_i \quad (9)$$

$$\frac{\partial^2 \mathbf{R}^{(2)}}{\partial \varphi^2} \mathbf{x}_i = \begin{bmatrix} 0 & 0 & 0 \\ 0 & -1 & 0 \\ 0 & 0 & -1 \end{bmatrix} \mathbf{x}_i \quad (10)$$

and \mathbf{x} as the vector of surface grid point locations.

3.3. Stiffness and Damping from Time Domain GAF Signals

The mechanical work of a system with hysteretic response to harmonic excitation may be considered as consisting of a contribution due to the system's stiffness (W_k) and one due to the system's damping characteristics (W_c) [24, 25]. The inclination and enclosed area of the hysteresis, as shown in Figure 3, are the parameters defining these work terms. Here, the fictional input signal $q(t)$ is plotted against time t in the bottom figure and the upper left figure shows the time history of the fictional output signal $Q(t)$. The top right figure displays the resulting hysteretic response. By focusing on the first harmonic content in the signals and evaluating the corresponding integrals, the normalized work terms become [26]

$$\frac{W_k}{\hat{q}^2} = \frac{1}{\hat{q}^2} \int_0^{\hat{q}} \frac{\hat{Q} \cos(\varphi)}{\hat{q}} q dq = \frac{1}{2} \frac{\hat{Q}}{\hat{q}} \cos(\delta) \quad (11)$$

$$\frac{W_c}{\hat{q}^2} = \frac{1}{\hat{q}^2} \int_T^{T+\frac{2\pi}{\omega}} Q \frac{dq}{dt} dt = \frac{\hat{Q}}{\hat{q}} \pi \sin(\delta) \quad (12)$$

with δ being the phase difference between output and input signal, T the period of oscillation, ω the angular frequency, and \hat{q} and \hat{Q} the magnitudes of input and output signal, respectively. In structural dynamics, the concept of a complex stiffness is commonly employed to describe the stiffness and damping characteristics with a single complex valued quantity, usually referred to as complex modulus. It consists of a real part, the mechanical storage stiffness, and an imaginary part, the mechanical

loss stiffness. The complex modulus is defined as

$$k^*(\omega) = k'(\omega) + jk''(\omega) \quad (13)$$

$$k'(\omega) = \frac{\hat{Q}}{\hat{q}} \cos(\delta) = \frac{2W_k}{\hat{q}^2} \quad (14)$$

$$k''(\omega) = \frac{\hat{Q}}{\hat{q}} \sin(\delta) = \frac{W_c}{\pi\hat{q}^2} \quad (15)$$

$k'(\omega)$ characterizes the stiffness property and $k''(\omega)$ the damping property. As both quantities are merely a scaling of the integrals described in Eq. 11 and 12, this concept is used in the present work to assess the aerodynamic stiffness and damping from harmonic forced excitations.

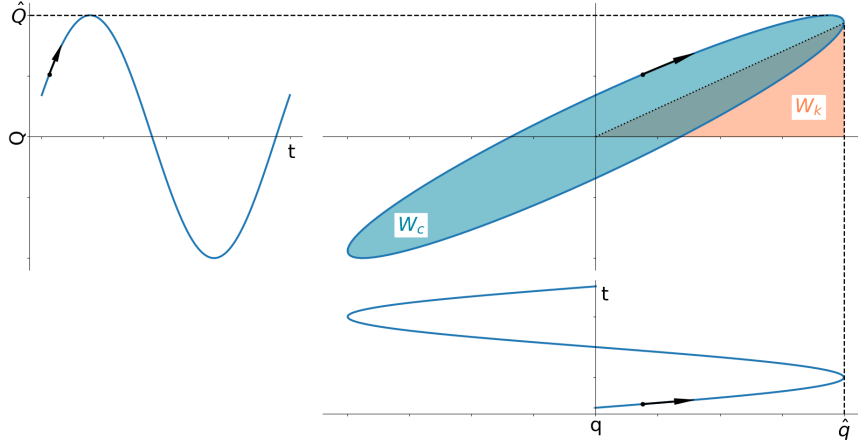


Figure 3 – Illustration for GAF hysteresis analysis

4. Simulation Model

The configuration studied in this work is the HTP of a generic T-tail configuration according to [5] (Figure 4). The lifting surface with a span of 8 m and a chord length of 2 m is unswept and untapered. In order to account for the effect of steady aerodynamic forces, an incidence angle of 3.0° is chosen, resulting in a steady lift coefficient of 0.216 at Mach 0.4 and atmospheric properties at mean sea level according to the International Standard Atmosphere [27]. The origin for the rigid body rotations of the HTP is located in the xz-plane with a distance of 6 m below the lifting surface and 0.5 m aft of its leading edge. The simplicity of the model facilitates a fast method development and provides an opportunity to gain a profound insight into the physics of T-tail flutter within short time. Furthermore, the model can easily be modified for parametric studies.

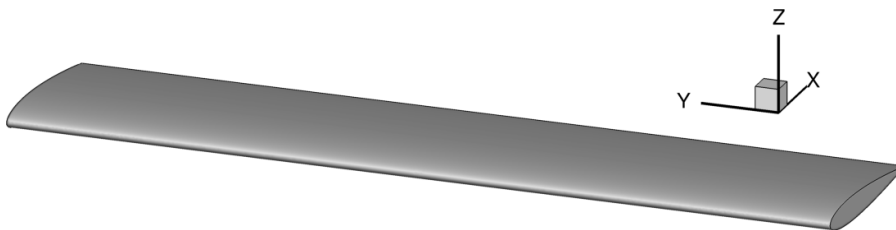


Figure 4 – HTP of the generic T-tail configuration

An unstructured mesh of the HTP for nonlinear, inviscid flow simulation is used for this study. The farfield covers 50 chord lengths in front, left, right, below, and above the configuration and 150 chord lengths aft of it. To ensure the results being independent of the spacial discretization, four mesh densities are considered (Table 1) and the generalized aerodynamic response to harmonic excitation at 5.0° roll angle amplitude and a reduced frequency of 0.231 is assessed w.r.t. the highest mesh density, which is referred to as “reference”. The resulting deviations in GAF magnitude and phase

angle are shown in Figure 5 for the influence of aerodynamic forces induced by HTP roll motion on the roll motion itself, $Q_{hh}(1, 1)$, and on the yaw motion $Q_{hh}(2, 1)$. Only the fine mesh shows deviations below 1.0% in magnitude and phase angle for both GAF terms and is used for studying the amplitude dependent characteristics of the GAF values.

Table 1 – Mesh densities used for mesh independence study

		coarse		medium		fine		reference	
No. grid points / 1e6	Factor	0.254	1.0	0.432	1.70	0.865	3.41	1.412	5.56
No. surface elements / 1e6	Factor	0.049	1.0	0.086	1.75	0.178	3.63	0.412	8.41
No. volume elements / 1e6	Factor	1.419	1.0	2.407	1.70	4.816	3.39	7.689	5.42

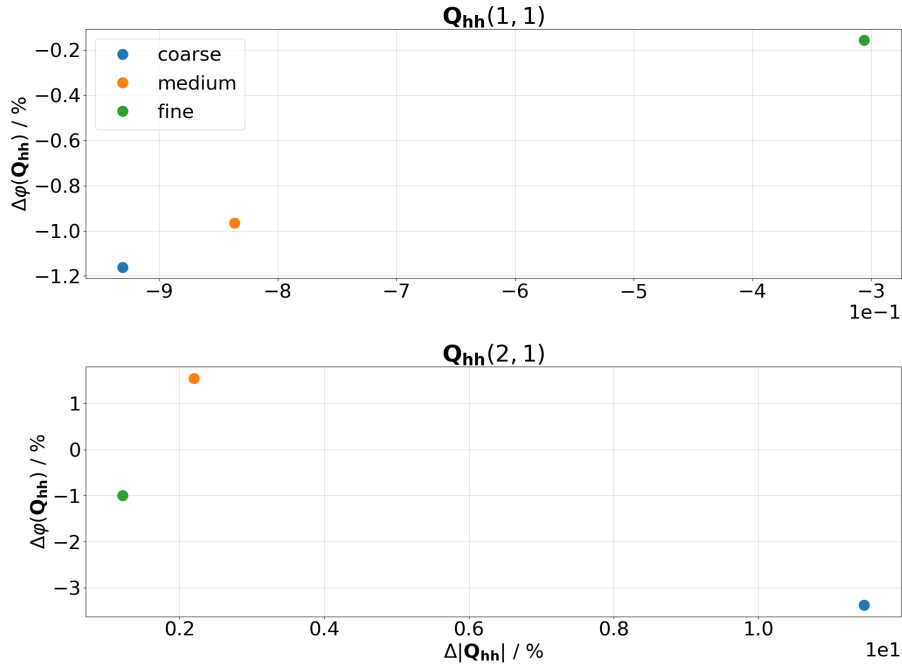


Figure 5 – Relative errors in GAF magnitude and phase angle for three mesh densities w.r.t. the reference mesh; linear deformation, 5.0° roll angle amplitude, reduced frequency 0.231

5. Results

5.1. Verification of GAF Computation Using LFD Results

Verification of the chosen approach for GAF computation from time domain signals is done by comparison of the first harmonic content with complex GAFs from LFD computations. As the comparison addresses only the postprocessing routine for the time domain simulations and does not depend on the mesh density, the coarse mesh is used to reduce computational time. The GAF magnitudes ($|Q_{hh}|$) and phase angles ($\varphi(Q_{hh})$) resulting from a linearized roll motion with a small roll angle amplitude of 0.01° are evaluated at increasing reduced frequencies, as illustrated in Figure 6. The plots show the results regarding the aerodynamic influence of the HTP roll motion on itself ($Q_{hh}(1, 1)$) and on the yaw motion ($Q_{hh}(2, 1)$). Four reduced frequencies (0.056, 0.090, 0.146, 0.231) are selected for the time domain simulations (TD). For the highest reduced frequency, the time step size yields 100 time steps per period of oscillation. The harmonic oscillations are carried out with a time step size of 0.002 s and continued until the magnitudes of the two GAF values obtained from a sliding Fourier transform show a residual of 0.1% for a time span of two periods. With this approach, the resulting magnitudes and phase angles of the first harmonic GAF content from time domain results show an excellent agreement with the LFD results, confirming the selected approach.

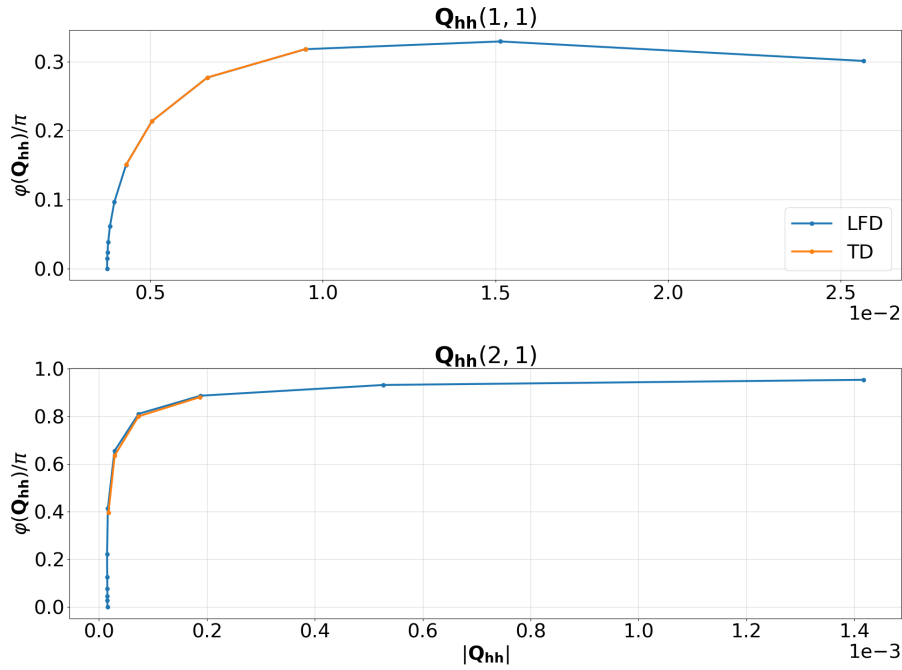


Figure 6 – Comparison of magnitude ($|Q_{hh}|$) and phase angle ($\varphi(Q_{hh})$) of first harmonic GAF content between LFD and time domain (TD) approach for the aerodynamic influence of linear HTP roll motion on roll and yaw motion

5.2. Generalized Aerodynamic Response to Harmonic Excitation

The simulation results presented below are based on the fine mesh and cover the low reduced frequency of 0.056 together with the high reduced frequency of 0.231 as well as the amplitudes 0.010° , 0.917° , 1.834° , 3.669° and 5.000° . Taking fully nonlinear deformations as a basis, these amplitudes correspond to relative deformations of the center of the HTP w.r.t. the VTP span of 0.017%, 1.600%, 3.200%, 6.403% and 8.724%, respectively. The largest deformation amounts to roughly 0.6 m at the HTP tip. Figure 7 summarizes the GAF response over sinusoidal motion input in roll and yaw for increasing amplitudes and reduced frequency values k . The aerodynamic influence of the HTP roll motion on itself and on the yaw motion, $Q_{hh}(1, 1)$ and $Q_{hh}(2, 1)$, is illustrated in Figures 7a and 7c, respectively. The aerodynamic influence of the HTP yaw motion on the roll motion and on itself, $Q_{hh}(1, 2)$ and $Q_{hh}(2, 2)$, is depicted in Figures 7b and 7d, respectively. For all figures, the reduced frequency is increased from top to bottom, whereas the results based on linear and quadratic deformation are displayed from left to right. The input signal and the response are normalized to the deformation amplitude.

Figure 7a shows largely coinciding ellipsoids with regard to the deformation amplitude for the diagonal GAF term $Q_{hh}(1, 1)$. A distinct impact of the nonlinear deformation term on the inclination of the hysteresis is notable, even for smallest amplitudes. The elliptical shape of the hysteresis does not change considerably with amplitude.

Contrary to the observations made for $Q_{hh}(1, 1)$, the inclinations of the hystereses of $Q_{hh}(2, 1)$ shown in Figure 7c are only marginally affected by higher order deformation terms, but their shapes and enclosed areas are. For linear deformations, a distinct higher order term in the aerodynamic response is notable, which is reduced with quadratic deformation components. However, a deviation of the hystereses from an elliptical shape with increasing deformation amplitude can still be identified for quadratic deformations at high reduced frequencies.

Insensitive to the deformation description is the aerodynamic coupling term $Q_{hh}(1, 2)$, Figure 7b. For both, linear and quadratic deformation, a small reduction in inclination with increasing deformation amplitude can be noticed. For all reduced frequencies and amplitudes, the hystereses maintain their elliptical shape.

Similar to the first diagonal GAF term, the second diagonal term $Q_{hh}(2, 2)$ shows a change in inclination for all amplitudes and reduced frequencies when higher order deformation terms are taken into

account. However, the hystereses coincide for all deformation amplitudes.

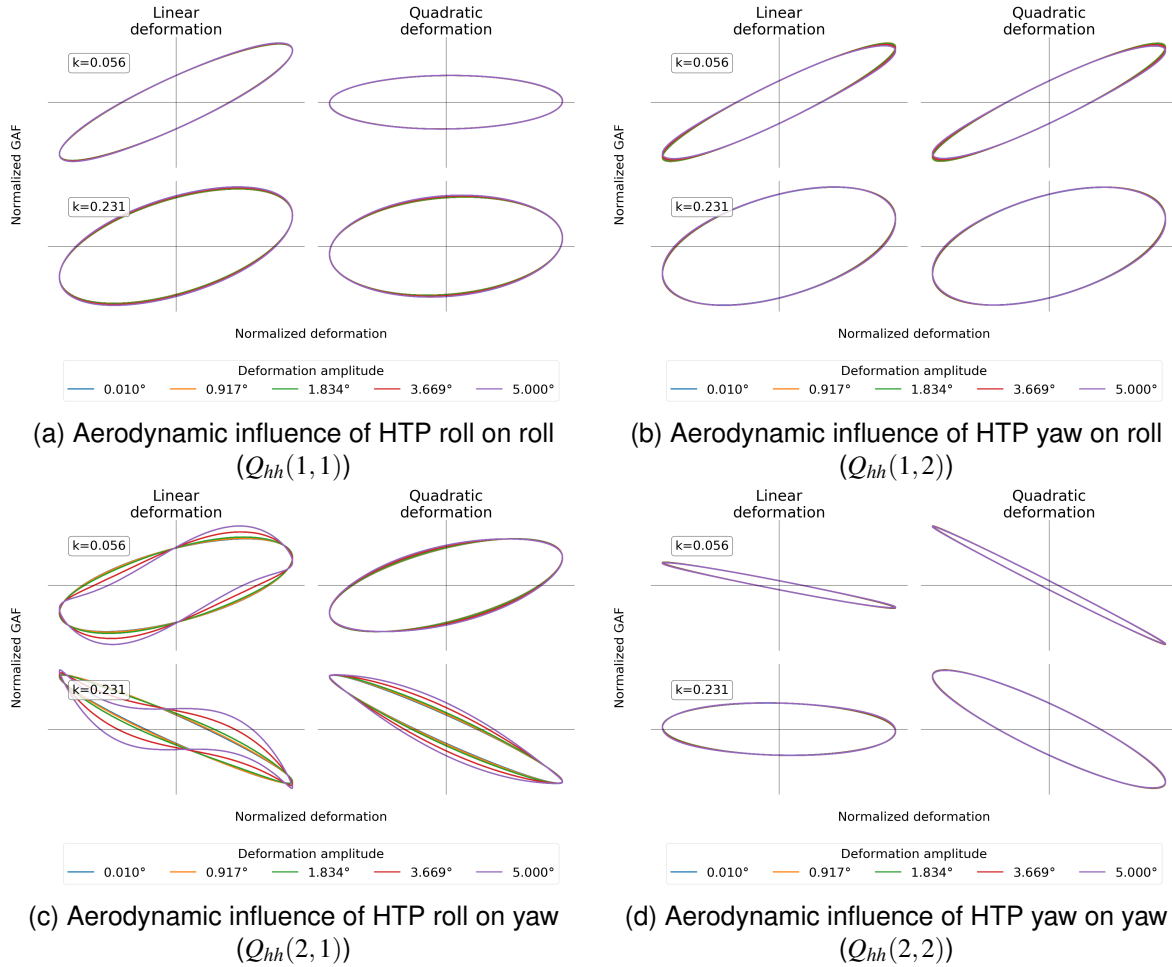


Figure 7 – Generalized aerodynamic response to harmonic excitation

With the approach outlined in section 3.3, the storage and loss stiffness values are evaluated in terms of relative deviations to the values for linear deformation at smallest amplitude, as this represents the values used for linear flutter assessment. In the following, the terms storage stiffness and aerodynamic stiffness will be used interchangeably, as will the terms loss stiffness and aerodynamic damping. Since all GAF terms appear to be rather insensitive to the deformation amplitude, the analysis will be focused on GAF term $Q_{hh}(2, 1)$. Figure 8 shows the storage and loss stiffness values over deformation amplitude evaluated for the first harmonic term in the GAF signal. The linear deformation approach is represented by the blue solid line, while the orange solid line illustrates the results based on quadratic deformation. For small amplitudes, the linear and quadratic deformations yield identical stiffness and damping values for all reduced frequencies. Ramping up the deformation amplitude reveals a nonlinear dependency of the aerodynamic stiffness (left figure column) with a sign change between linear and quadratic deformations. While an increase in stiffness for small reduced frequencies is observable for the linear deformation, the quadratic deformation actually indicates a decrease in stiffness, which is significantly lower in magnitude compared to the linear deformation. At large reduced frequencies, the effect is reversed and the linear deformation shows a reduction in stiffness up to 15% at 5.0° deformation amplitude. With quadratic deformation components, an increase in stiffness is observable, but again considerably lower in magnitude compared to the change in stiffness based on linear deformations. The impact of the higher order deformation components on aerodynamic damping (right figure column) is again a sign change for low reduced frequencies. The linear deformations result in a slight reduction in damping, whereas the quadratic deformation terms yield an increase in damping with a higher magnitude. At large reduced frequencies, both deformation approaches show a distinctly nonlinear dependency of the damping on the deformation amplitude with deviations exceeding 40% for the largest deformation amplitude. Here, the quadratic

deformation approach results in a larger impact on the damping compared to the linear one. The essential observations may be summarized as follows:

- Aerodynamic stiffness (i.e. storage stiffness)
 - Nonlinear for low and high reduced frequencies with linear deformations
 - Marginally nonlinear for low and high reduced frequencies with quadratic deformations
 - Sign change between linear and quadratic deformation
- Aerodynamic damping (i.e. loss stiffness)
 - Marginally nonlinear for low reduced frequencies with sign change between linear and quadratic deformation
 - Nonlinear for high reduced frequencies without sign change between linear and quadratic deformation

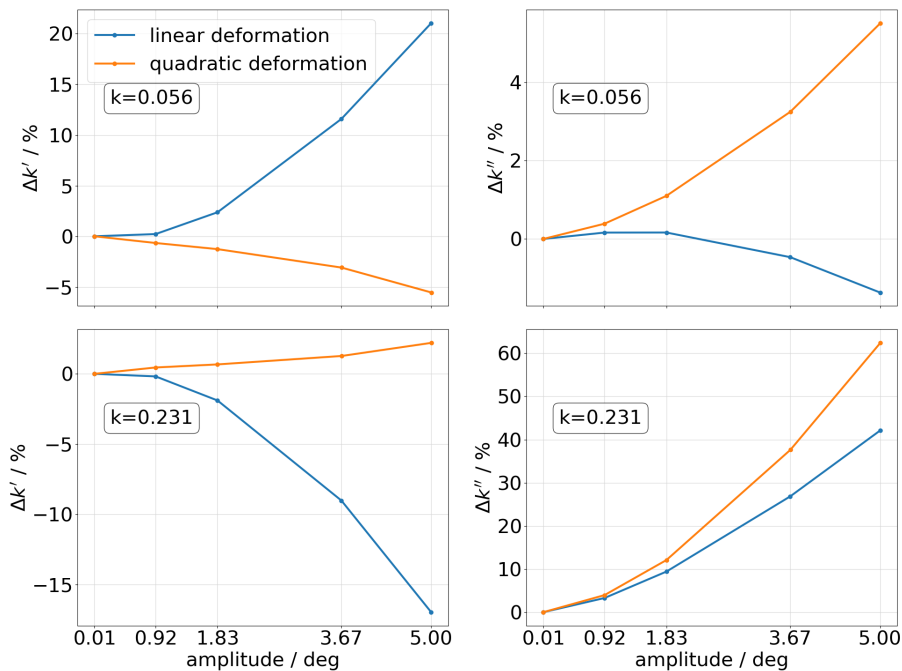


Figure 8 – Storage and loss stiffness values over amplitude for $Q_{hh}(2, 1)$

6. Discussion

Evident from the hysteretic response of GAF term $Q_{hh}(2, 1)$, Figure 7c, is a third harmonic content for linear deformations. As the excitation of the system comprises only a first harmonic term, the higher harmonic component in the generalized response is attributed to the induced aerodynamic forces only. In order to identify the physical source for this nonlinearity, the normalized GAF values at each CFD surface node are computed for 0.01° and 5.0° roll angle amplitude at a reduced frequency value of 0.231. For a linear system with an independent response to the excitation amplitude, the difference between the normalized responses amounts to zero. This is not the case for the studied HTP undergoing roll motion, which is visualized in Figure 9. Here, the differences in GAF magnitude are computed between the surface values at large and small deformation amplitude, followed by subtraction of the values at the lower surface from the upper surface. The results are displayed in Figure 9a for the longitudinal and in Figure 9c for the lateral force components with linear deformations. Clearly, a nonlinearity can be observed at the wing tips, which leads to the assumption that induced drag forces are at least partly responsible for the amplitude dependent GAF response. The lateral force component reveals a distributed nonlinearity along the spanwise direction with an increase in magnitude closer to the wing tips. These contributions to the aerodynamic work presumably result

from the tilting of the steady aerodynamic force vectors in combination with the symmetric lateral displacements due to the yaw deformation.

The same analysis is made for the simulations based on quadratic deformations to address the impact of the higher order terms used for the deformation description on the nonlinear response, see Figure 9b and Figure 9d. The impact of the quadratic deformation components on the nonlinearity in the longitudinal generalized aerodynamic forces, as a comparison of Figure 9a with Figure 9b reveals, appears to be negligible, but the one regarding the lateral forces reveals a distinct difference, cf. Figure 9c and Figure 9d. The nonlinear contributions close to the tips remain, but the distributed nonlinearity along the spanwise direction is reduced considerably. This observation is explicitly illus-

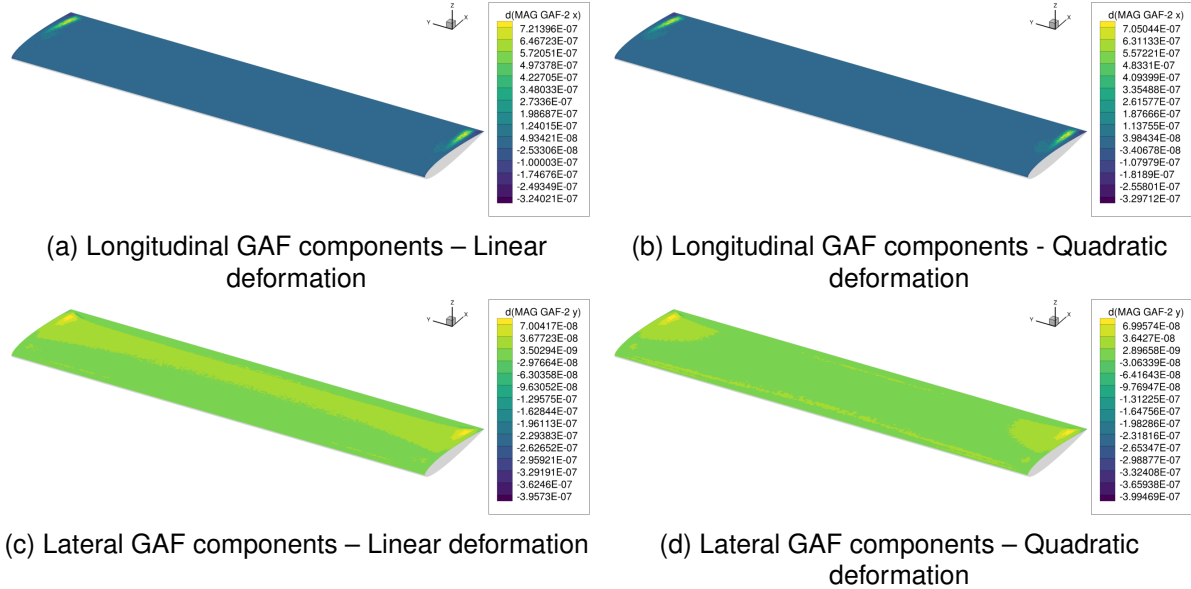


Figure 9 – Deviations in normalized GAF magnitude for $Q_{hh}(2,1)$ between 5.0° and 0.01° roll deformation amplitude; reduced frequency value 0.231

trated in Figure 10 for a slice along the spanwise direction at 75 % chord and one along the chordwise direction at 96.25 % semi-span. Using quadratic deformation components for the surface mesh deformation and the generalization of aerodynamic forces distinctly reduces the nonlinear character of the lateral aerodynamic force components, as evident from Figure 10a. The nonlinear character of the longitudinal as well as the lateral aerodynamic force components at the wing tip is, however, insensitive to the deformation description, see Figure 10b. This directly implies that the extended modal approach needs to be employed for the study of amplitude dependent T-tail flutter, as the effect of the higher order terms is not restricted to the mechanical work of the aerodynamic forces induced by the HTP roll motion performed on the HTP roll motion itself, but is also evident for the mechanical work performed on the HTP yaw motion apart from smallest deformation amplitudes. That is, the aerodynamic coupling term is nonlinear w.r.t. the deformation amplitude, but fundamentally different between a linear and a nonlinear deformation approach.

The source for the amplitude dependent response is encircled to the unsteady induced drag components and to the lateral aerodynamic forces. To address their relevance for the stiffness and damping, the time domain GAFs are evaluated as outlined above, but with an individual artificial linearization of the longitudinal and lateral force components, respectively. For reduced frequency values of 0.056 and 0.231, the resulting hystereses are shown in Figure 12. By comparing Figure 11a with Figure 7c, it can be seen that the higher harmonic component in the GAF signal is eliminated when the longitudinal force components are linearized. That is, the induced drag component introduces a higher order term in the generalized aerodynamic response to harmonic excitation when a linear structural deformation is employed. A linearization of the lateral force components, as a comparison of Figure 11b with Figure 7c reveals, does not affect the higher order GAF term.

By analyzing the hystereses in terms of storage and loss stiffness values of their first harmonic content and comparing the resulting values with those based on nonlinear aerodynamic forces, as

NONLINEARITIES IN GAF IN THE CONTEXT OF T-TAIL FLUTTER

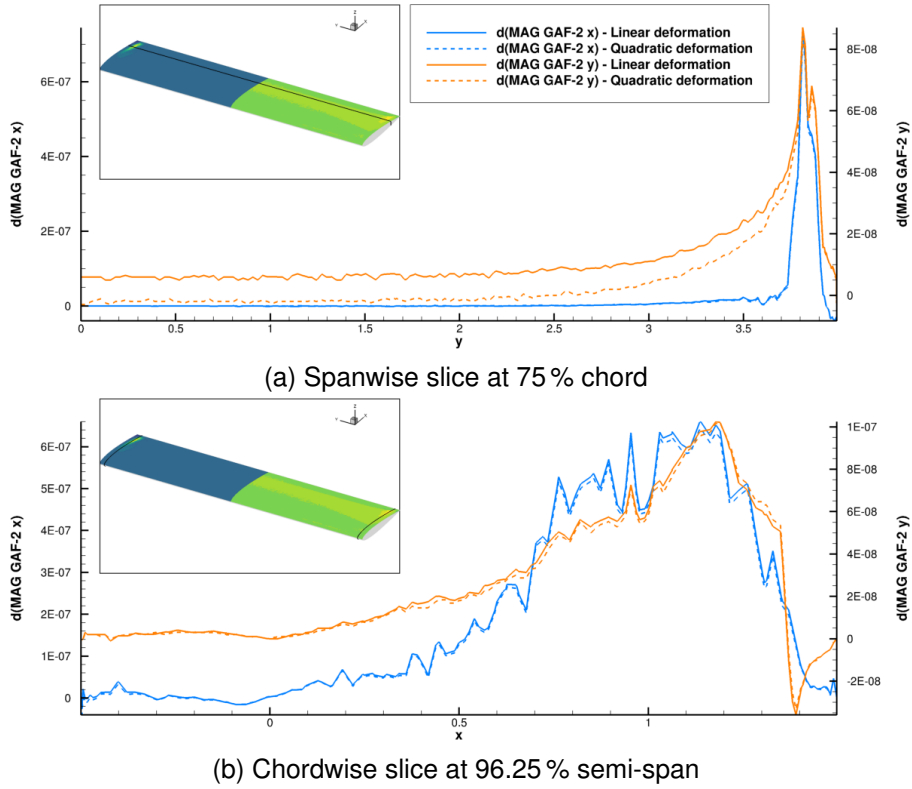


Figure 10 – Spanwise and chordwise deviations in normalized GAF magnitude for $Q_{hh}(2, 1)$ between 5.0° and 0.01° roll deformation amplitude; linear and quadratic deformation, reduced frequency value 0.231

shown in Figure 12, the longitudinal force components f_x are identified to be mainly responsible for the stiffness nonlinearity. With a selective linearization of these force components (dashed lines), the stiffness nonlinearity is reduced distinctly. A linearization of the lateral force components f_y (dotted lines) appears to have a major influence on the damping nonlinearity. However, the nonlinearity in the longitudinal forces is also not negligible for the damping.

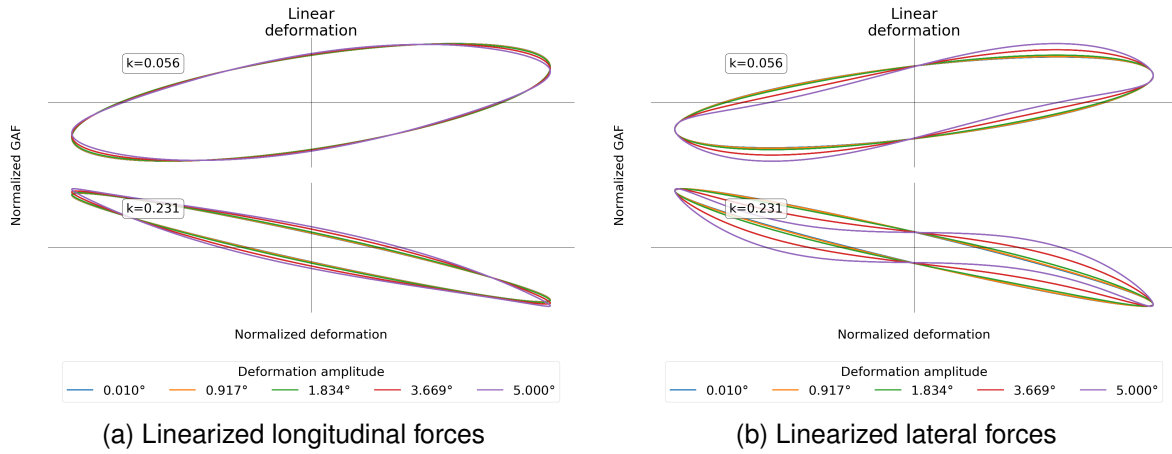


Figure 11 – Impact on hystereses of $Q_{hh}(2, 1)$ by artificial linearization of longitudinal and lateral force components; linear deformation

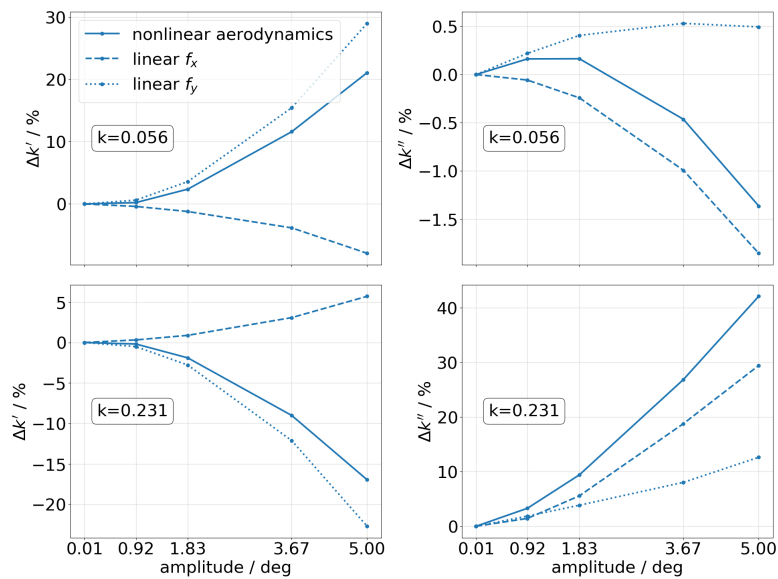


Figure 12 – Impact on loss and storage stiffness values of $Q_{hh}(2, 1)$ by artificial linearization of longitudinal and lateral force components; linear deformation

7. Conclusion and Outlook

Firstly, the present work affirms the necessity to take into account nonlinear deformations when dealing with T-tail flutter studies in combination with unsteady aerodynamic forces from CFD methods or DLM enhancements. Literature has already indicated this for the stiffness of VTP out-of-plane bending flexibility, i.e. the HTP roll motion in a broader sense. Beyond that, this work has demonstrated its relevance for the stiffness of the HTP yaw motion as well, which represents the VTP torsion flexibility. However, the simulation model does not feature a VTP and, hence, the aerodynamic forces due to torsion of the VTP itself are not accounted for. These might reduce the relevance of the higher order terms for the stiffness of the diagonal GAF term. Additionally, the response of the aerodynamic forces to harmonic excitation at various deformation amplitudes and reduced frequencies is shown to be largely linear w.r.t. the deformation amplitude, except for the aerodynamic coupling terms. Here, especially the aerodynamic influence of HTP roll motion on HTP yaw motion (i.e. VTP out-of-plane bending on VTP torsion) reveals a strong nonlinearity in stiffness and damping, which is shown to be dependent on the higher order deformation terms used for the description of the surface mesh deformation. In particular, the nonlinearity in stiffness is reduced significantly with higher order deformation terms. Contrary, the damping nonlinearity of this term is amplified. Apart from this, a third harmonic term in the generalized aerodynamic response can be identified at high deformation

amplitudes and linear deformations, which is reduced when quadratic deformation components are included. However, apart from identifying the physical source for this effect to be related to longitudinal force components, it is not further examined in this work. As nonlinear deformations are already required for reasonable linear T-tail flutter assessment, the nonlinearity observed for the coupling terms may be relevant for nonlinear dynamic effects, e.g. Limit Cycle Oscillations (LCOs). Hence, using a linear modal structural model for the study of nonlinear T-tail flutter seems inappropriate.

Two physical sources for the aerodynamic nonlinearity are identified, which comprise longitudinal aerodynamic forces due to induced drag and lateral aerodynamic forces from HTP roll. While the first nonlinear term is concentrated near the HTP tips and independent of the deformation description, the latter one shows a distribution in spanwise direction over the entire lifting surface with an increase near the HTP tips. With quadratic deformation terms included in the simulations, the nonlinearity of the lateral forces is reduced to contributions near the wing tips. Hence, a strong sensitivity to the higher order deformation terms in the form of a reduced nonlinearity in GAF magnitude with higher order deformation terms is observed.

The current studies are limited to inviscid flow at a subsonic Mach number, but the observed nonlinearity is shown to be sensitive to longitudinal forces. Hence, fluid viscosity and compressibility could reveal further insight into the character of this nonlinearity, for which reason future studies will comprise a similar approach but with viscous forces included in the governing fluid equations at subsonic and transonic Mach numbers. In addition, the study uses uncoupled quadratic mode shape components for the extended modal approach. If the roll motion of the HTP showed a small yaw component, which would be the case for VTP out-of-plane bending and torsion with non-collinear mass and elastic axes, it would be required to take into account coupled quadratic mode shape components, as they directly affect the off-diagonal terms in the equation of motion. In order to conclusively make a point regarding the actual impact of the observed nonlinearity on amplitude dependent T-tail flutter stability, it is aspired to introduce a small coupling into the rigid body mode shapes and study the stability of the system by time marching free deformation simulations.

8. Copyright Statement

The authors confirm that they, and/or their company or organization, hold copyright on all of the original material included in this paper. The authors also confirm that they have obtained permission, from the copyright holder of any third party material included in this paper, to publish it as part of their paper. The authors confirm that they give permission, or have obtained permission from the copyright holder of this paper, for the publication and distribution of this paper as part of the AEC proceedings or as individual off-prints from the proceedings.

References

- [1] W. P. Jennings and M. A. Berry. "Effect of Stabilizer Dihedral and Static Lift on T-Tail Flutter". In: *Journal of Aircraft* 14.4 (Apr. 1977), pp. 364–367.
- [2] E. Suciu. *MSC/Nastran Flutter Analyses of T-Tails Including Horizontal Stabilizer Static Lift Effects and T-Tail Transonic Dip*. Presented at the 1996 MSC/Nastran World Users' Conference. June 1996.
- [3] E. Suciu et al. *A DLM-Based MSC Nastran Aerodynamic Flutter Simulator for Aircraft Lifting Surfaces*. MSC.Software 2013 Users' Conference. May 2013.
- [4] L. van Zyl and E. H. Mathews. "Aeroelastic Analysis of T-Tails Using an Enhanced Doublet Lattice Method". In: *Journal of Aircraft* 48.3 (2011), pp. 823–831. DOI: 10.2514/1.C001000. URL: <http://dx.doi.org/10.2514/1.C001000>.
- [5] J. Murua, L. van Zyl, and R. Palacios. "T-Tail flutter: Potential-flow modelling, experimental validation and flight tests". In: *Progress in Aerospace Sciences* 71 (2014), pp. 54–84.
- [6] H. Arizono, H. R. Kheirandisch, and J. Nakamichi. "Flutter simulations of a T-tail configuration using non-linear aerodynamics". In: *International Journal for Numerical Methods in Engineering* 72.13 (2007), pp. 1513–1523.
- [7] A. Attorni, L. Cavagna, and G. Quaranta. "Aircraft T-tail flutter predictions using computational fluid dynamics". In: *Journal of Fluids and Structures* 27.2 (2011), pp. 161–174.

- [8] K. Isogai. "Subsonic and Transonic Flow Simulation for an Oscillating T-Tail - Effects of In-plane Motion of Horizontal Tail Plane -". In: *Transactions of the Japan Society for Aeronautical and Space Sciences* 59.1 (2016), pp. 25–32.
- [9] K. Isogai. *Numerical Simulation of Transonic Flutter of a T-Tail*. International Forum on Aeroelasticity and Structural Dynamics. June 2017.
- [10] E. Santos et al. "Development of a CFD-based industrial procedure for supporting the aircraft certification with application to A400M T-Tail flutter". In: *Second International Symposium on Flutter and its Application*. 2020.
- [11] D. J. Segalman and C. R. Dohrmann. *Dynamics of rotating flexible structures by a method of quadratic modes*. Tech. rep. Sandia National Labs., Albuquerque, NM (USA), 1990.
- [12] C. R. Dohrmann and D. J. Segalman. *Use of quadratic components for buckling calculations*. Tech. rep. Sandia National Labs., Albuquerque, NM (United States), 1996.
- [13] D. J. Segalman and C. R. Dohrmann. "A method for calculating the dynamics of rotating flexible structures, part 1: Derivation". In: *Journal of Vibration and Acoustics* 118.3 (July 1996), pp. 313–317. ISSN: 1048-9002. DOI: 10.1115/1.2888183. eprint: https://asmedigitalcollection.asme.org/vibrationacoustics/article-pdf/118/3/313/5625518/313_1.pdf.
- [14] D. J. Segalman, C. R. Dohrmann, and A. M. Slavin. "A method for calculating the dynamics of rotating flexible structures, part 2: Example calculations". In: *Journal of Vibration and Acoustics* 118.3 (July 1996), pp. 318–332. ISSN: 1048-9002. DOI: 10.1115/1.2888184. eprint: https://asmedigitalcollection.asme.org/vibrationacoustics/article-pdf/118/3/318/5625621/318_1.pdf.
- [15] R. Robinett et al. *Flexible Robot Dynamics and Control*. Vol. 19. Springer Science & Business Media, 2002. DOI: 10.1007/978-1-4615-0539-6.
- [16] M. R. Ritter. "An extended modal approach for nonlinear aeroelastic simulations of highly flexible aircraft structures". PhD thesis. Technische Universität Berlin, 2019.
- [17] L. van Zyl and E. H. Mathews. "Quadratic Mode Shape Components From Linear Finite Element Analysis". In: *Journal of Vibration and Acoustics* 134.1 (2012). DOI: 10.1115/1.4004681.
- [18] J. Farao, A. G. Malan, and F. Gambioli. "Towards a Non-Linear Full Aircraft Model For Passenger Aircraft Loads Calculations". In: *International Forum Aeroelasticity and Structural Dynamics, Como, Italy* (2017).
- [19] Dominik Schäfer. "T-tail flutter simulations with regard to quadratic mode shape components". In: *Deutscher Luft- und Raumfahrtkongress* (2020).
- [20] Sebastiano Fichera and Sergio Ricci. "High order harmonic balance applied to an aeroelastic T-tail model with a control surface freeplay". In: *American Institute of Aeronautics and Astronautics*. 2013.
- [21] Sebastiano Fichera and Sergio Ricci. "Freeplay-induced limit-cycle oscillations in a T-tail: numerical vs experimental validation". In: *Journal of Aircraft* 52.2 (2014), pp. 486–495. DOI: <https://doi.org/10.2514/1.C032748>.
- [22] R. Thormann. "Accurate and Efficient, Time-linearized Flutter Analysis of Transport Aircraft". PhD thesis. TU Braunschweig, 2018.
- [23] I. N. Bronstein et al. *Taschenbuch der Mathematik*. 10th ed. Verlag Harri Deutsch, 2016.
- [24] M. Wahle. *Maschinendynamik*. Vorlesungsmanuskript FH Aachen. 2008.
- [25] Giancarlo Genta. *Vibration dynamics and control*. Springer, 2009.
- [26] Cyril M. Harris and Allan G. Piersol. *Harris' shock and vibration handbook*. McGraw-Hill New York, 2002.
- [27] National Oceanic and Atmospheric Administration (US). *US standard atmosphere, 1976*. Vol. 76. 1562. National Oceanic and Atmospheric Administration, 1976.